J Neurosurg 97:119–128, 2002

Failure of single-unit neuronal activity to differentiate globus pallidus internus and externus in Parkinson disease

STEVEN J. SCHIFF, M.D., PH.D., BRIAN K. DUNAGAN, AND ROBERT M. WORTH, M.D., PH.D.

Krasnow Institute for Advanced Study and Department of Psychology, George Mason University, Fairfax, Virginia; Department of Electrical Engineering and Computer Science, Massachusetts Institute of Technology, Cambridge, Massachusetts; and Department of Neurosurgery, Indiana–Purdue University, Indianapolis, Indiana

Object. The authors examine the validity of single-unit neuronal recordings as a method of differentiating the globus pallidus internus (GPi) from the GP externus (GPe) in Parkinson Disease.

Methods. One hundred twenty-eight recordings of apparent single-unit activity used to help guide final electrode placement in eight patients who underwent pallidotomy were analyzed using sophisticated spike sorting methods, and 185 neurons were characterized for mean firing frequency and percent of firing within bursts. In addition, the total spectral power was calculated on the full measured waveform for each of 128 samples without spike sorting. No correlation was identified between these measures of neuronal activity and depth within the GP.

Conclusions. These results call into question the validity of relying on single-unit activity and microelectrode recordings in the operating room to localize lesion or electrode placement within the GPi during stereotactic pallidal surgery.

KEY WORDS • Parkinson disease • globus pallidus • single-neuron response • microelectrode

THE GP is a complex structure; it can be partitioned into the GPe and the GPi, whose major efferents project to the subthalamic nucleus (from the GPe), and to the thalamus and midbrain (from GPi).[5] Two years after Spiegel, et al.,[14] reported improvement in a small number of patients with PD in whom stereotactic lesions were made in the pallidum and ansa lentiformis, Svennilson, et al.,[16] reported marked improvement in patients with PD who underwent a more refined lesion of the GP. Following renewed interest in pallidotomy first communicated by Laitinen, et al.,[9] in 1992, placement of stereotactic pallidal lesions in the GPi with electrophysiological microelectrode assistance to delineate its boundaries has now become common in many centers.

In 1971, DeLong[4] made the observation that in awake monkeys *(Macacca mulatta)* at rest, distinctive differences in the discharge patterns of neurons in the GPi compared with the GPe were observed. Two types of neurons were identified in the GPe: one had recurrent periods of high-frequency discharge with relatively silent periods in between, and the other was characterized as having a low-frequency discharge with bursts (similar to sample D in Fig. 1). In contrast, in the GPi only one type of neuron was identified, a continuously discharging cell without long periods of silence (similar to sample C in Fig. 1). Border cells from the pallidal segments were characterized by regular firing (similar to sample B in Fig. 1).

These observations in normal macaque monkeys have been used as the physiological foundation for microelectrode recording to increase the precision of stereotactic electrode placement within the GPi in humans undergoing lesioning or electrode placement for PD. Multiple centers report using DeLong's findings to distinguish the GPi from the GPe.[1,7,10,15,18,19] Unfortunately, each of the diverse patterns recorded in Fig. 1, although displaying features that should help the surgeon localize GPe, GPi, and border cells, were recorded from sites within 1.2 mm of each other deep within the anatomical GPi of a single patient. Such findings motivated the critical analysis that follows.

The only way to ensure that physiological recordings are indeed from single neurons within the brain is to impale a single neuron with a sharp or patch-type microelectrode. This is technically difficult in intact animals, and is not feasible in humans because of the hazards associated with using glass micropipette electrodes; therefore, one generally resorts to extracellular recordings of neuronal activity obtained using metal microelectrodes. Such recordings are customarily an amalgam of the activity produced by multiple nearby neurons, and spike extraction and sorting techniques are required to isolate the sequence of spikes from single neurons, which are also called single units.

Abbreviations used in this paper: AC–PC = anterior commissure–posterior commissure; GP = globus pallidus; GPe = GP externus; GPi = GP internus; MR = magnetic resonance; PD = Parkinson disease.

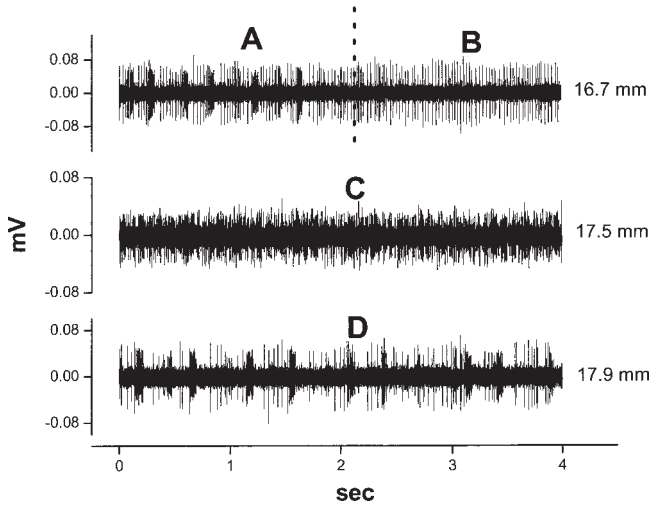

FIG. 1. Three 4-second samples of microelectrode recordings obtained in the patient in Case G. The first tracing, Sample A, shows high-frequency bursts and singlet firing, which spontaneously change into regular firing throughout the longer tracing, of which this is a short example. The latter half of the first tracing, Sample B, was typical for border cells on the pallidal boundaries as defined by DeLong. Sample C is typical of the continuously high-frequency discharging cells that should populate the GPi. Sample D shows low-frequency discharges with bursts, as should be seen in the GPe. Each of these tracings, however, was recorded from deep within the anatomical GPi, from locations within 1.2 mm of each other. The trajectory depth measurements, specified to the right of each example, are measured from a zero value assigned at 15 mm above the AC–PC plane. Therefore, all of these measurements, which fall between 16.7 and 17.9 mm, are well within the anatomical GPi. Not only are cells supposedly representative of each of the regions of the pallidum found clustered together, but the qualitative nature of the cells (for example, from bursting to regular firing) are seen to change spontaneously as a given electrode position is monitored (Samples A/B). Calculated values for Samples A through D are cross-referenced in the corresponding panels in Figs. 6 and 7, which show results in the patient in Case G.

Traditionally, such spike sorting would be performed by photographing the individual spike waveforms from an oscilloscope display, and examining which spikes overlapped precisely in outline when projected using a photographic enlarger onto tracing paper. The advent of modern digital recording methods and more advanced computers has permitted a vast improvement in the ability to handle large numbers of spike-sorting comparisons, but sophisticated waveform morphology studies and cluster analysis are required to try to substitute for the human ability to perform the visual task of grouping and overlapping individual spike waveforms.[20]

The DeLong[4] study was performed without spike sorting, and the applications to human electrode localization have almost always been done without the benefit of such methods. Complicating the issue is the fact that surgical decisions are made on the fly in the operating room, which although not excluding sophisticated spike analysis, has generally precluded more than a cursory inspection of amplitude tracings with the assistance of a threshold trigger (generally spike peak amplitude), and an audio monitor for the surgeon to listen to, which provides frequency information. Several reports of primate neuronal single-neuron responses in the GPe compared with the GPi after 1-methyl-4-phenyl-1,2,3,6-tetrahydropyridine treatment have been published, but again, no effort at spike sorting was reported.[6,12] We are aware of one report in which spike threshold discrimination, and some spike sorting, was performed off-line on data obtained in humans, but it is unclear how often and to what degree waveform discrimination was applied to the data sets.[7] Even when some postsurgical data processing was performed, there appears to be no confirmation of overlap of spike waveform morphological features in this literature, and no cluster analysis, ensuring a high degree of confidence that single units were indeed correctly identified. Examples of uncertainty in single unit identification are pervasive in the literature, and can be seen in Fig. 1 from Sterio, et al.,[15] Fig. 2 from Hutchinson, et al.,[7] Figs. 1 and 3 from Lozano, et al.,[10] and even the classic data from Fig. 1 of DeLong.[4]

In this study we examine the data collected during eight routine microelectrode procedures, and apply state of the art spike detection, extraction, and sorting to permit neuronal characterization of GPe and GPi cells. We are unable to correlate neuronal firing characteristics with anatomical location within the GP.

Materials and Methods

Data Collection

Data were collected in eight patients ranging in age from 56 to 77 years, who underwent pallidotomy for symptoms of PD. Patients discontinued all their antiparkinsonian drugs at 8:00 the night before surgery and had thus been off medication for approximately 16 hours by the time recording began. Microelectrode recording was performed with the GS3000 system (Axon Instruments, Foster City, CA), after placement of the 80% platinum/20% iridium glass-insulated microelectrodes. The impedance of these electrodes, measured at 1 kHz in brain tissue, averaged 0.63 MΩ (range 0.46–0.83 MΩ). Stereotactic targeting of the GP was performed using both direct and indirect MR imaging methods. For the direct method, the GPi was identified using fast spin–echo inversion-recovery axial MR imaging, the target was selected in the posteromedial corner on the slice passing through the AC–PC plane, and the target was cross-confirmed on the corresponding coronal image. Indirect targeting was also performed with reference to the AC–PC line according to published coordinates.[9,10,15,17] The results were cross-referenced to those of the direct method. The mean initial coordinates were 2.5 mm anterior to the midcommissural point, 21 mm right or left laterally from the midline, and in the AC–PC plane. The stereotactic arc system coordinates were set to access this point and a guide tube was inserted along this trajectory to a position 15 mm above the selected target. Microphysiological recording was then begun at this point. Neurons from the GPe and GPi were recorded at 20 kHz over 12 bits of analog-to-digital resolution after high-pass single-neuron filtering at 300 Hz and low-pass antialiasing filtering at 5 kHz.

The depth at which neurons were identified within the GP was noted, and multiple parallel trajectories were performed in each patient to differentiate the boundaries of the GPi from the GPe. The boundary between the GPi and the internal capsule was defined by its decreased cellularity. Six patients underwent five recording passes and two underwent four passes. The passes were continued in the vertical direction until cellular activity ceased, which indicated the bottom of the GPi. Typically this occurred 5 to 6 mm below the AC–PC plane. In addition to localizing the GP, the recording passes were used to identify its posteromedial border with the internal capsule.

Once a likely lesion site had been identified, macrostimulation was performed using the lesion electrode at 100 Hz, with a 0.2-msec pulse duration, to assess the proximity to the optic tract and internal capsule. Evidence of photopsiae or sensorimotor symptoms below a

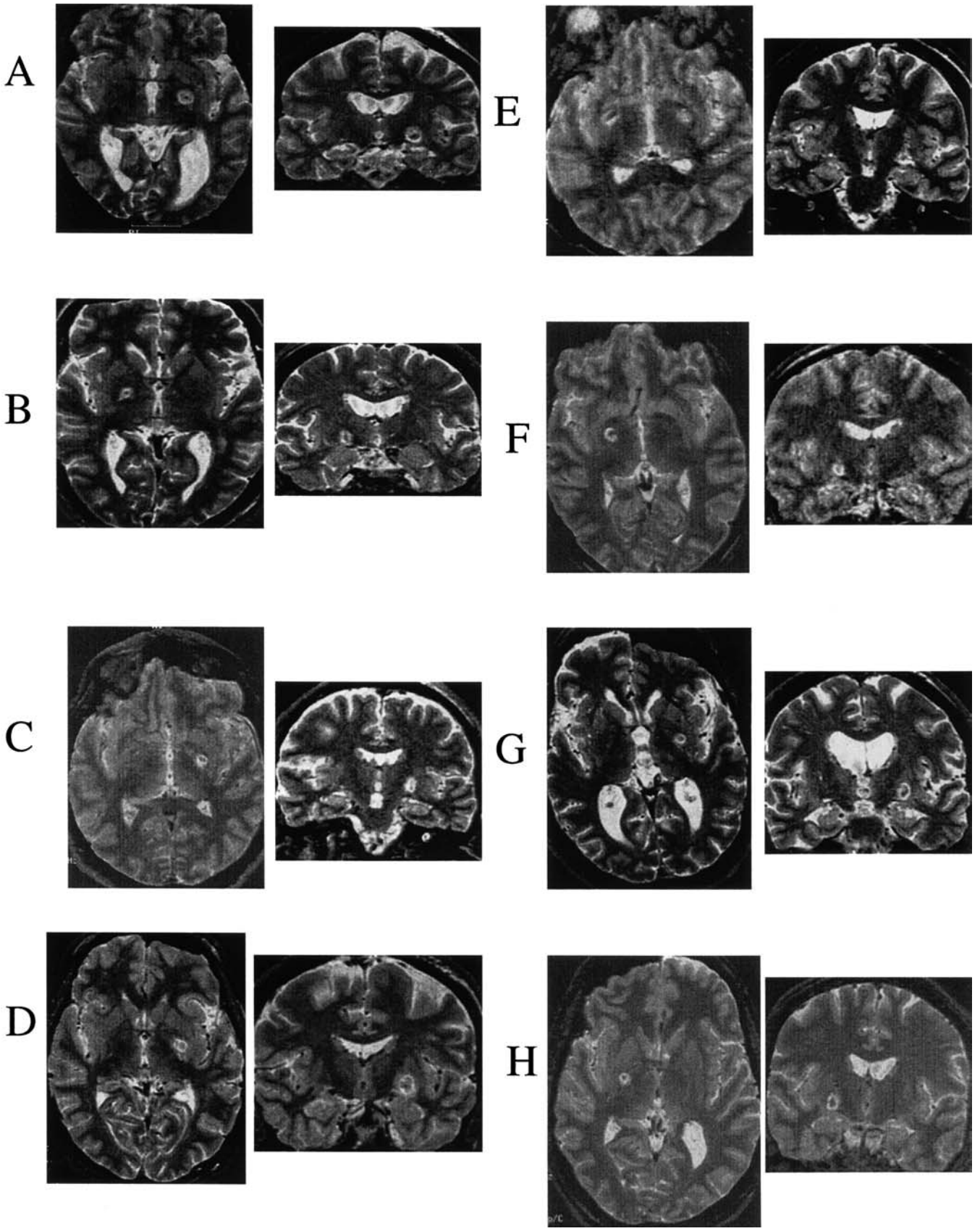

FIG. 2. Postoperative axial and coronal MR images obtained in all eight patients (Cases A–H), demonstrating GPi lesions.

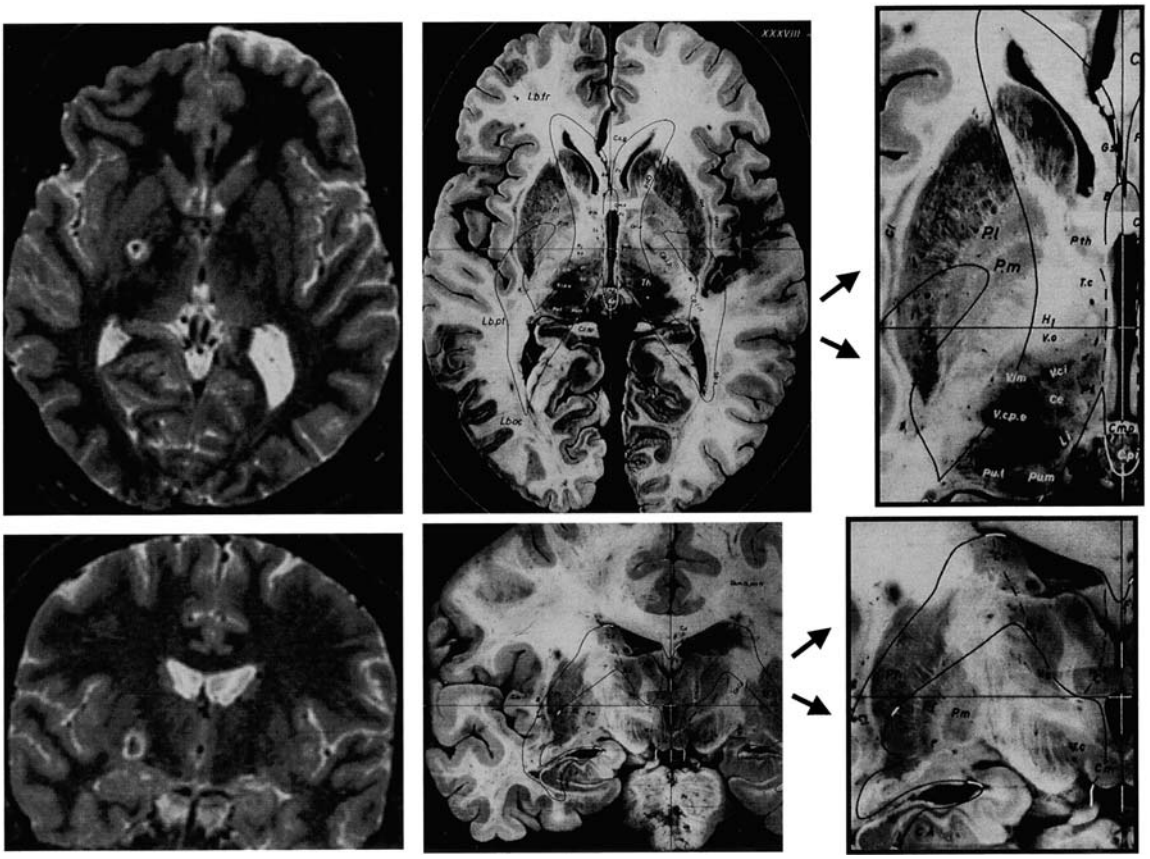

FIG. 3. Magnified postoperative MR image demonstrating the GPi lesion in the patient in Case H shown in axial and coronal views in the *left* panels. The *center* panels are from a standard atlas (Schaltenbrand and Wahren, reproduced with permission, Thieme Medical Publishers), with magnified details shown on the *right* panels, which correlate the lesion in this patient with the posteroventral region of the pars lateralis (P.l) and pars medialis (P.m) of the GPi.

current threshold of 3 μA was believed to indicate an unsafe location, and no lesion was made at that point. One patient had a single lesion, five had two, and two had three lesions. The mean lesion coordinates for the lower pole were 21.5 mm lateral and 3.5 mm anterior to the midcommissural point axially, and 3.25 mm below the AC–PC plane coronally, whereas the mean upper pole was 1 mm above the AC–PC plane coronally.

Lesion locations for all eight patients are illustrated in the postoperative axial and coronal MR images in Fig. 2. In Fig. 3, corresponding images from an atlas[13] are juxtaposed against the MR images obtained in the patient in Case H. The axial image is in the AC–PC plane, and the coronal image is just anterior to the midcommissural point; the lesion is within the posteroventral portion of the GPi, which is divided into the pars medialis and the pars lateralis.

Although this investigation was not performed primarily to assess the efficacy of the procedure, which has been well documented in other publications, some information regarding the outcome of these specific patients is relevant to the issue of targeting. One of the patients has not returned for follow-up evaluation. Six of the remaining seven patients had definite improvement in their parkinsonian symptoms, as measured 1 to 6 months postoperatively by a neurologist who was not involved in the surgery. The seventh patient had only questionable improvement, but had become so restless during the lengthy surgical procedure that only a partial lesion placement could be performed (Case B).

The spike-sorting analysis conducted in this study was performed on archived data analyzed after the surgical procedures had been completed, and did not influence surgical decisions in any way. This research was performed with approval from the Institutional Review Boards of both the Indiana–Purdue University and George Mason University, with an exemption (Category 4) for research on archived data.

Segments of data consisting of 10 to 90 seconds of microelectrode readings, were analyzed using the Common Processing Analysis software system from DataWave Technologies (Longmont, CO), and single-neuronal-unit extracellular spikes were detected and extracted. Clustering based on spike morphology was performed using Autocut analysis software from DataWave Technologies. Each neuronal spike was extracted from a microelectrode tracing by using custom-set thresholds for each particular data set, using a threshold crossing (positive or negative), and a slope peak at threshold crossing (positive or negative going derivative of the voltage with time) to identify candidate spikes. Each candidate spike was extracted with 1 msec of voltage recording before and after the threshold detection point, to give a short 2-msec sample for further analysis. The goal in spike extraction was to capture all the spikes from the dominant neuron in a tracing, which generally corresponded to the one with the largest peak amplitude. Almost always, several other neurons were seen to contribute to such a collection of extracted spikes.

The extracted spikes, which are embedded in their 2-msec windows of recording, are then compared with eight different features of waveform morphology, as follows: 1) maximum peak amplitude of the waveform from zero-voltage deflection (peak); 2) absolute minimum of the waveform from zero voltage (valley); 3) time at which the peak occurred (measured relative to the start of the 2-msec extracted trace); 4) time at which the valley occurred; 5) difference between the peak and valley amplitudes (total spike height); 6) difference between the peak and valley time (spike width); 7) ratio of the peak/valley areas; and 8) ratio of the peak/valley amplitudes. These quantities were projected into a 32-dimensional parameter space, and

a nonlinear clustering technique was used to fit elliptical boundaries to clusters. Clusters are defined by the distance in this space from each spike's point to the center of the nearest potential cluster, and the cluster points are required to fall within 2.5 standard deviations of the mean of the cluster. Once cluster boundaries were chosen statistically, all clustered spikes were individually overlapped and visually inspected. No automatic spike-sorting algorithm can substitute for human judgment, and clustering parameters and weighting were adjusted if necessary to be able to extract at least one clean neuron, which we call the primary neuron in this study. Often, a second neuron could be cleanly extracted, and these were also analyzed. In many tracings more than two neurons were visible, and in these cases, all neurons not classified as the primary or secondary neuron were labeled as unclassified.

The mean rates of firing for all identified neurons were calculated, and interspike interval histograms were constructed. To quantitate the percentage of spikes occurring as bursts for a given neuron, we have used the percentage of interspike intervals lasting less than 8 msec, which is the burst criterion most commonly used in neurophysiological studies to delineate bursting neuron activity in the superior colliculus,[11] striate cortex,[3] and middle temporal extrastriate cortex (MT or V_5).[2] Auto-correlations and cross-correlations were calculated for the primary, and, when available, secondary spikes, but were not used in the subsequent analysis.

The total power per second of the tracings was calculated by computing the power spectral density of every 4096 (2^{12}) data points, which corresponded to 0.2048 seconds of data recorded at 20 kHz. These values were converted into units of power per second for each window, and the average of all the nonoverlapping windows required to cover the data set were computed. Each data set was inspected visually before power analysis to exclude regions of signal artifact that would have contributed spurious measurements to the overall average. Because there was a wide variation observed in the power values, logarithms were calculated to facilitate comparison. For occasional tracings (20 of 128), the gain of the recording system was changed to accommodate exceptionally large-amplitude spikes. Although this gain alteration had no effect on spike extraction and clustering, it made the total power analysis uncertain, and these 20 tracings were excluded from the total power comparisons.

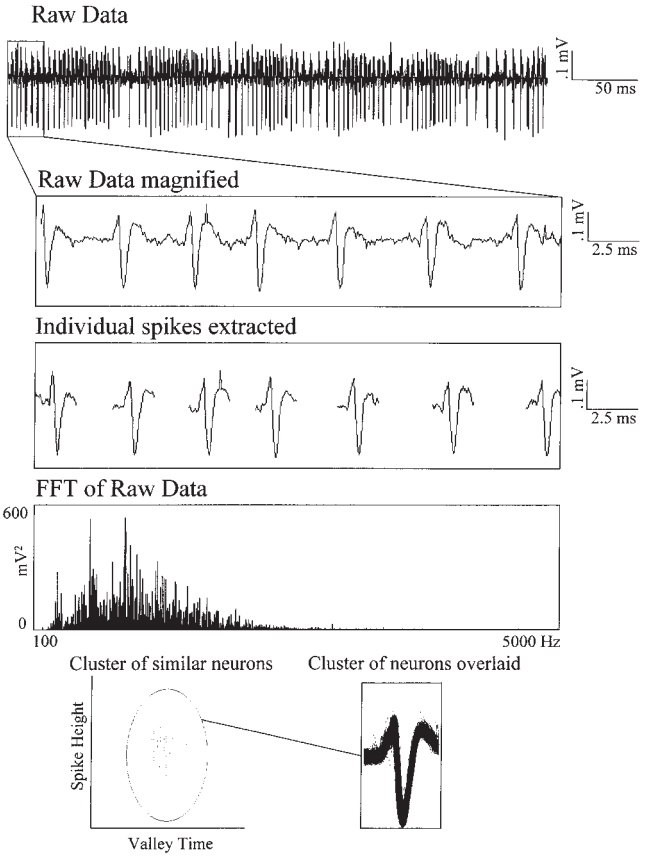

FIG. 4. Sample E of microelectrode recording of raw data obtained in the patient in Case A, first panel. The second panel shows raw data at an expanded time scale, with details of neighboring spikes. The third panel shows the results of spike detection and extraction; only a 2-msec (ms) segment of data is retained and centered on the threshold crossing point for spike detection. The fourth panel shows a power spectrum (squares of the absolute values of the fast Fourier transform [FFT]) of the entire sample of raw data. The total power for this sample is obtained by summing the values in the power spectrum. In the fifth panel, on the *left* is a projection of the 32-dimensional cluster analysis into a two-dimensional space, showing the comparison between spike height and valley time, and at the *right* is the overlap of all these clustered spikes in the same 2-msec window. These spikes meet the criteria for single units. Calculated values for Sample E are cross-referenced in the corresponding panels for this patient in Figs. 6 and 7.

Results

We analyzed 128 recordings for the presence of identifiable single-neuron units; 185 neurons were identified, 131 of which were primary and 54 of which were secondary neurons.

Figure 4 illustrates an example of data that contained a well-defined single unit, Sample E. In the upper two panels, segments of raw data are shown at two different time scales. Substantial variation is seen in the peak amplitudes in the upper trace.

The third panel in Fig. 4 illustrates the process of spike detection and extraction. Here, a threshold is set (positive or negative, depending on the tracing), with a minimum and maximum dwell time imposed following threshold crossing to eliminate noise spikes and voltage excursions too broad to be produced by single neurons (typical window settings were 0.1–1 msec for minimum and maximum dwell times). The extracted spikes are cut out in short 2-msec tracings, as shown in the third panel. Cluster analysis confirmed that these waveforms are a single unit. In the lower left of Fig. 4, a two-dimensional projection of spike height compared with valley time is shown with a single cluster of points. In the lower right of Fig. 4, each of the waveforms corresponding to the clustered points are overlapped. The high degree of overlap of waveform morphological features is characteristic of data from single units recorded at fine resolution ($\geq$ 10 kHz). Without such a detailed morphological analysis, it would be impossible to be certain that this tracing represents a single neuron.

Figure 5 shows a data segment from a different patient, Sample F. Here, the raw data might also be thought to belong to a single unit; certainly the differences in peak amplitude were comparable with that of the data in Fig. 4. Nevertheless, a detailed examination of the spike morphologies in the second and third panels shows that they are quite different. The cluster analysis shows that the peak and valley times now sort into several distinct clusters, from which at least two neurons can be cleanly extracted. These two neurons have very different morphologies, and the overlapped waveforms in the insets confirm the validity of the cluster

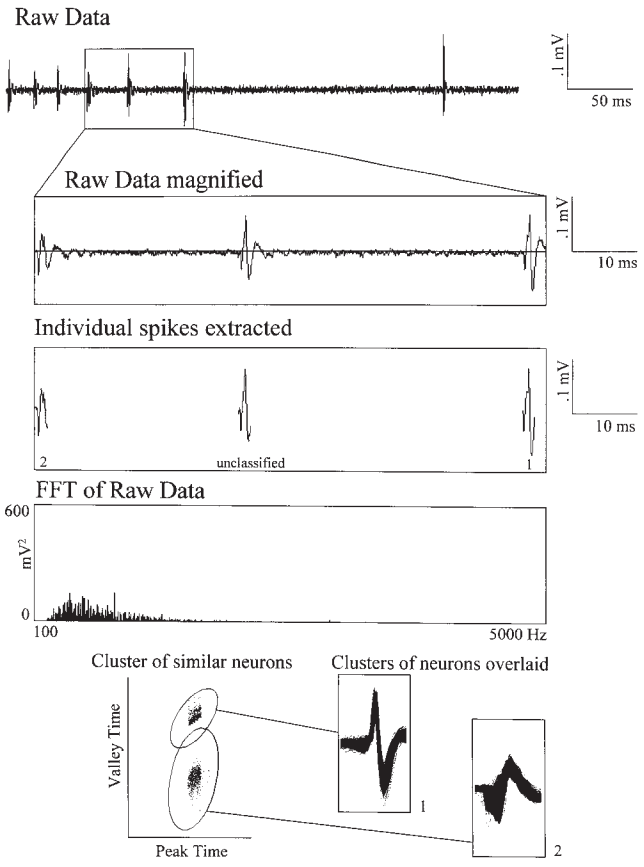

FIG. 5. Sample F showing similar analysis for a microelectrode recording as in Fig. 4, but in the patient in Case F. The rate of spike firing is less, but the spikes at increased time resolution (second panel) have different shapes. The extracted spikes (third panel) fall into two distinct clusters in the *left* of the fifth panel, with unclassified spikes falling outside the cluster boundaries (not shown). The spikes from these two clusters overlap with two quite distinctive morphologies, confirming the validity of the cluster analysis. The power spectral analysis shown in the fourth panel reflects less total power in this tracing compared with the more active tracing from Fig. 4. Calculated values for Sample F (neurons 1 and 2) are cross-referenced in the corresponding panels for this patient in Figs. 6 and 7.

analysis. There were many spikes that fell outside of these two main clusters, and these neurons were all grouped as unclassified. The unclassified neurons undoubtedly represent many neurons in this tracing (one of which is labeled in the third panel), in addition to labeled examples of the primary neuron (1), and the secondary neuron (2). Only a sophisticated analysis of spike wave clustering allows us to distinguish between these different neurons. Visual examination of such data during surgery gives only the aggregate rate of the largest neurons depicted.

The mean frequencies and percentages of burst firing of all neurons were plotted as a function of depth within the GP in Fig. 6. Sequential trajectories ($\leq$ five per patient) were indicated by the symbol sequence of circles, squares, triangles, multiplication signs, and pluses. The zero point for calibrating the depth measurements was arbitrarily set 15 mm above the MR-selected target, that is, 15 mm above the AC–PC plane for each patient, and once the zero point was set it was fixed for all parallel tracts used for that patient. Thus, the neuronal activity as a function of depth can be compared across trajectories, although due to the irregularities of the borders of GPi compared with GPe, the electrode may not remain in the nuclei for all trajectories at a given depth. Nevertheless, if single-neuron activity correlates with anatomical location, a scatterplot of activity compared with relative depth within the GP should reveal changes in activity as a function of depth.

Figure 6 illustrates the mean frequency (Hz) and the burst frequency (percentage of interspike intervals $<$ 8 msec) for all neurons, including the primary, and, where available, the secondary extracted neuron as well. Unclassified neurons were not analyzed. Data points corresponding to neurons from Fig. 1 (Samples A–D), Fig. 4 (Sample E), and Fig. 5 (Sample F) are labeled in these scatterplots. At 17.5 mm in the patient in Case G, Sample C from Fig. 1, the sample closest to the continuous high frequency expected from GPi, has two neurons (C:1 and C:2) clearly contributing to the combined signal. Furthermore, the neuron from Fig. 4 (Sample E), is clearly firing at a higher rate than the neurons from Fig. 5 (Samples F:1 and F:2), and the burstlike quality of the raw data from the neuron in Fig. 4 is clearly evident in the high burst firing percentage for Sample E. There is no reliable relationship between either mean frequency or burst firing as a function of depth in any of these patients.

The most accurate single-neuron extraction in any attempt at spike sorting is always the largest one, what we call the primary neuron in this study. Perhaps the lack of correlation of activity with depth shown in Fig. 6 was due to the fact that when data from more than the primary neuron were included in these data sets, the accuracy of the spike timings for secondary neurons was decreased, and so the frequencies and burst percentages for these secondary neurons degraded the overall analysis. Figure 7 shows a similar analysis to Fig. 6, but this time only the primary neurons were used. Unfortunately, we again failed to identify patterns that indicate reliable correlation of depth with neuronal activity when only primary neurons were analyzed. Although isolated examples could have been chosen to demonstrate the utility of such data (such as the mean frequency plots from the patient in Case A, or the burst frequency from the patient in Case C), in which a linear regression would quantify the significant change in activity with depth, no pattern emerges with enough consistency to be a basis for surgical judgment.

If single-neuron activity does not correlate well with anatomical depth, perhaps we should consider the entire measured neuronal activity in aggregate. Although sorting single neurons becomes progressively less accurate as one attempts to extract more and more neurons from a single electrode recording, we could measure aggregate activity of all of the contributing neurons near the electrode by a measure of the total power in the signal. Total power or energy in a signal can be equivalently estimated from the original voltage as a function of time by summing the squared values of voltage deflection within a time window, or, in the frequency domain, by computing the sum of the power spectral density within a time window. We selected the latter method because the fast Fourier transform facilitates this computation. In Figs. 4 and 5, the fourth panels show the power spectrum calculated on the samples of raw data in

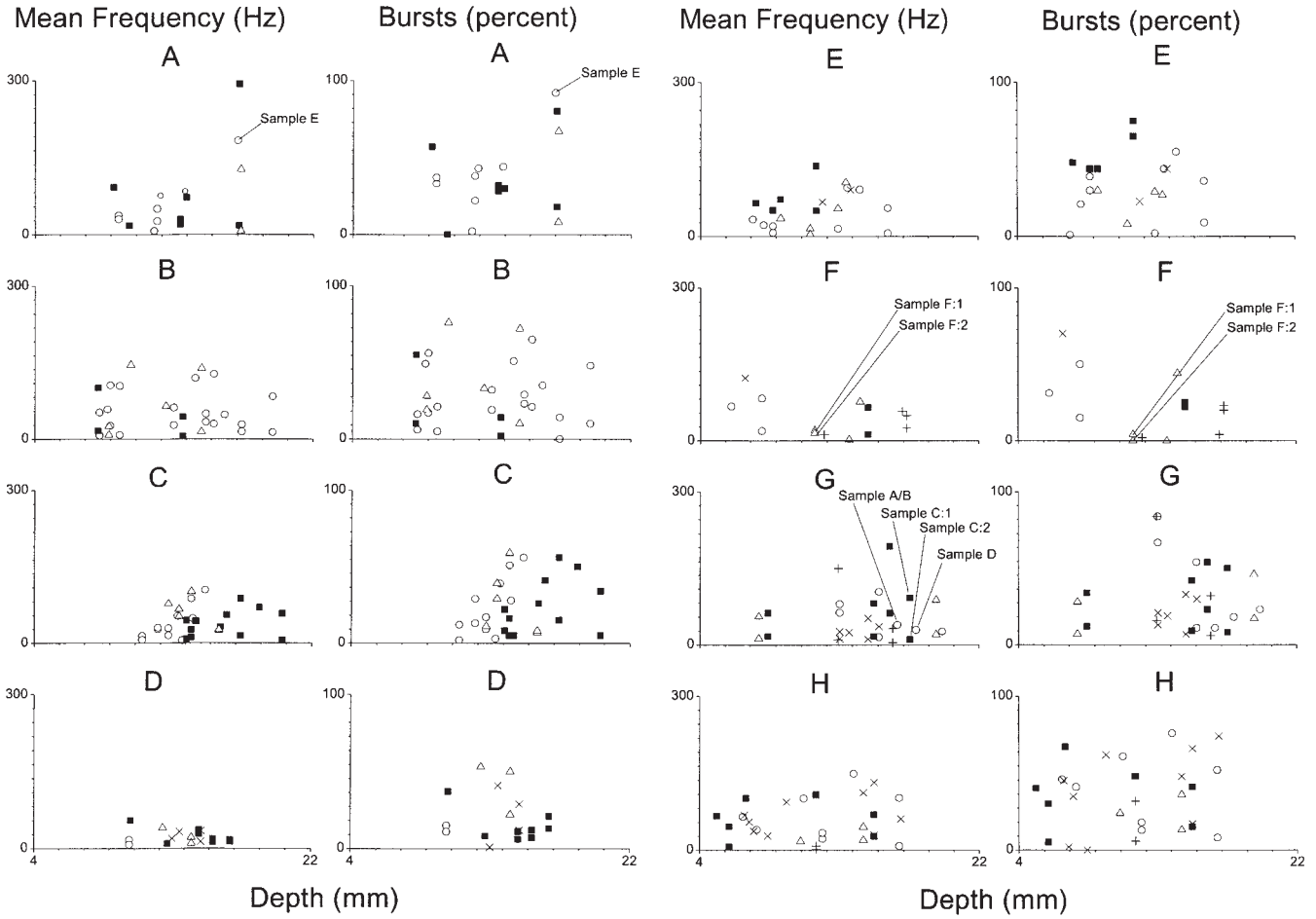

FIG. 6. Scatterplots showing a comparison of mean frequency (Hz) and bursts (percentage of interspike intervals < 8 msec) as a function of depth within the GP for all identified neurons in all eight patients (Cases A–H). The points corresponding to the mean rate and burst percentages of Samples A through D from Fig. 1 are indicated. Sample C from Fig. 1 has two neurons (C:1 and C:2) contributing to the aggregate rate. The higher mean rate and burst percentage from Sample E compared with the two Sample F neurons (F:1 and F:2) are clearly evident. No correlation between these measures and depth within the GP can be seen in any of the eight patients. Symbols indicate sequential trajectories (up to five per patient) in the following order from first to last: circles, squares, triangles, multiplication signs, and pluses.

the first panels. These figures show that the total power (sum of all spectral density values) is clearly higher for Sample E than for Sample F, reflecting the greater amount of neuronal activity in Sample E.

Figure 8 shows the logarithm of the average total power per second for each recording. In this plot, the raw data tracing was broken up into 0.2048-second windows, and the total power was calculated for each window and then averaged over all windows in a given tracing. No differentiation between different neurons is performed here, so there is only one scatterplot for each patient. Again, no correlation between this measure of aggregate neuronal activity and depth of recording within the GP is observed.

Discussion

The analysis of microelectrode data can be complex. Not all such data require that the activity from single neurons be characterized, but such characterization frequently requires extensive and time-consuming analysis to extract and sort the waveforms from individual neurons.

Our findings were surprising to us, and arose in concert with a study of the ensemble dynamics of basal ganglia neurons. Recognizing that little if any single-cell work on PD had been performed with sophisticated spike clustering measures, and that routine microelectrode recording data obtained in the operating room might combine the activities from multiple neurons in a given tracing, we first examined the characteristics of the true single neurons that were accessible in our tracings. Although for a given threshold setting we could frequently extract two clean neurons, the actual number of extractable neurons in our tracings was often much greater, and could have been sorted using a combination of different thresholds to extract different spikes.

Because of our failure to correlate the activities of the ensemble of spikes with depth within the GP, we limited our analysis to just the largest or primary neuron in each tracing. This primary neuron is typically the one that would be recognized on an operating room monitor in which a peak

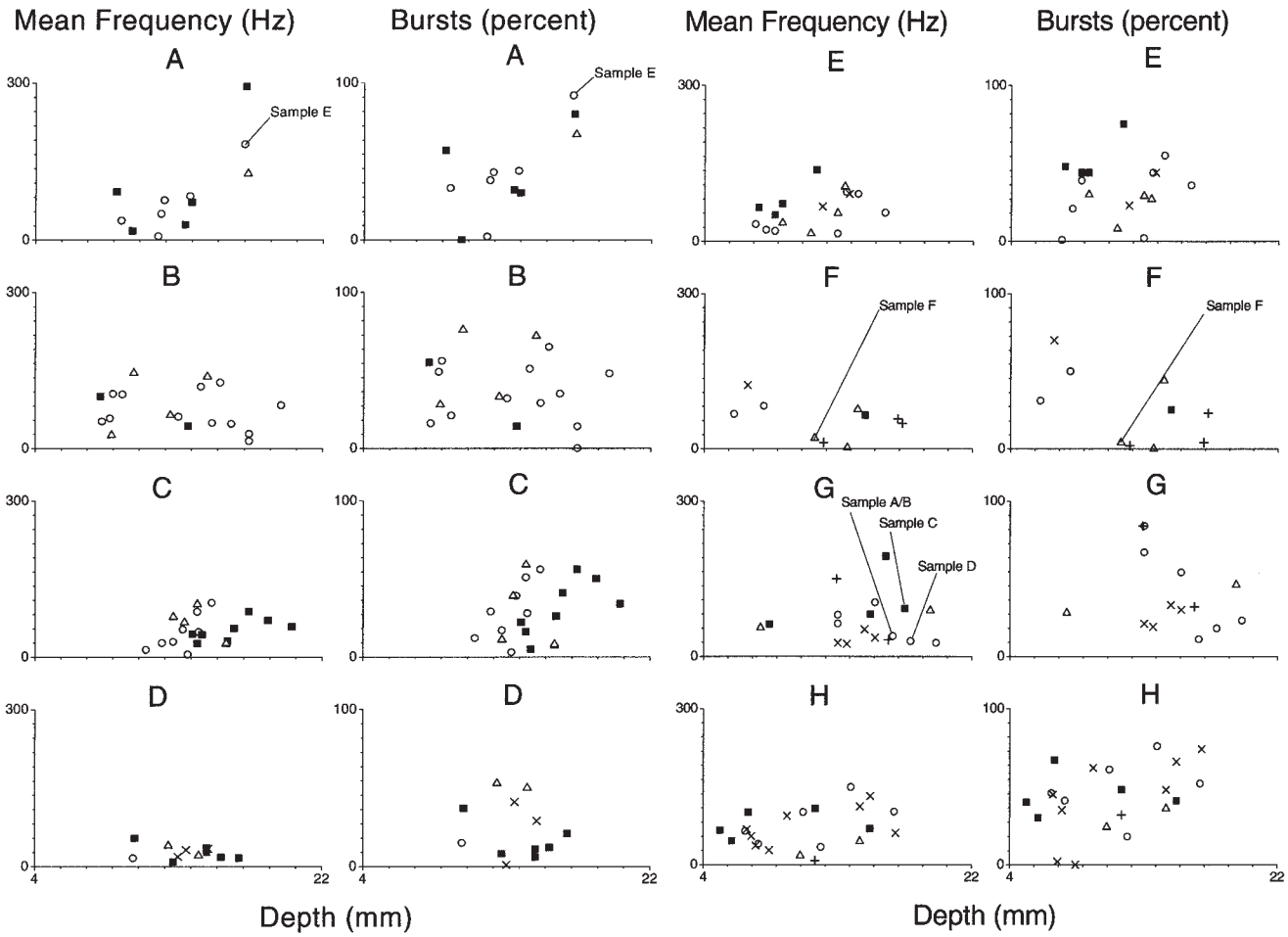

FIG. 7. Scatterplots showing a similar analysis to Fig. 6, except that only the data for the single primary neurons from each data set are shown. Again, no reliable correlation between these measures and depth within the GP is observed. See Fig. 6 for explanation of symbols.

threshold detector is used to trigger the display, and is the one that often dominates the audio monitor signal. Nevertheless, we failed to differentiate depth within the GP by using these data.

Finally, assuming that single-cell data were the wrong information on which to concentrate, we examined the full microelectrode recording, with all neurons included, in a total power analysis. Unfortunately, with this approach we also failed to correlate these measures with depth within the GP.

Our findings are in contrast with those in multiple experimental and clinical reports, all of which have suggested that the original experimental findings in monkeys could be observed in humans with PD. Nevertheless, we also note that the classic experimental primate descriptions were completed without the benefit of spike sorting analysis. The possibility therefore exists that some of the physiological foundation that supports modern microelectrode surgical procedures was based on multiple rather than single cells.

The issue is more than academic: if one is searching for the differentiation between a high-frequency cell with pauses, or a cell with burst firing, as is claimed for neurons within the GPe, and seeks to note the appearance of continuously firing cells within the GPi possessing considerable irregularity with frequent brief fluctuations in rate, such tracings could be easily observed when multiple intermittently firing or burst firing neurons contribute their respective activities to fill in the gaps in a microelectrode recording. Sample C from Fig. 1 is an example of a tracing showing high-frequency activity without gaps, yet more than one neuron contributed to this aggregate recording (Samples C:1 and C:2 in Fig. 6). Thus, localization without spike sorting, based on continuous rather than intermittent firing, or based on the rate of apparent firing, are misleading when tracings contain contributions from multiple neurons.

Is the audio amplification of the microelectrode signal helpful for the surgeon in refinement of localization? Although we were unable to confirm any correlation between total spectral power and depth, such a measurement does not exclude the possibility that increases and decreases in power within narrow frequency bands may exist without an overall change in total power. In addition, the surgeon's auditory perception may be tuned to very complex patterns within a signal that are not readily reflected in simple spectral band power. We are, however, very concerned that reliance on auditory perception from microelectrode record-

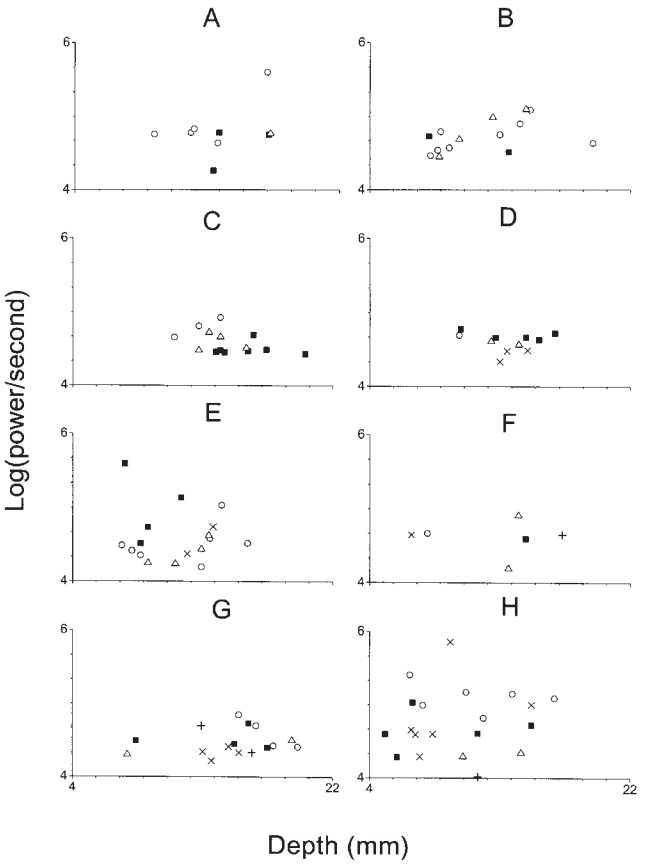

FIG. 8. Scatterplots showing the total average power from raw data. These measures are calculated by computing the power spectrum within all 0.2048-second windows from each data set, summing the values to get total power, and averaging these figures for all windows. The values represent a measure of total energy within the recording, and include contributions from all neurons firing without spike sorting. Again, no correlation between this measure and depth within the GP is observed. See Fig. 6 for explanation of symbols.

ings to delineate GPi boundaries may be fraught with potential subjective errors, and would be exceedingly difficult to standardize.

On the other hand, the benefits of modern pallidotomy, with and without microelectrode monitoring, have been demonstrated at multiple centers. The controversy over the use of microelectrode recordings for pallidal surgery was well reviewed by Alterman, et al.[1] Reports of successful posteroventral pallidotomy in patients with PD in whom less detailed microelectrode recordings were obtained, but in whom macrostimulation was used to delineate the locations of the optic tract and internal capsule have been published,[8] but no suitable objective study comparing pallidotomy with and without microelectrode recordings exists. If our findings are verified by others, one would have to consider the distinct possibility that the safety and efficacy of pallidotomy might derive more from MR imaging localization and micro- or macroelectrode stimulation than from the added benefits of microelectrode recording.

Nevertheless, setting aside issues related to spike sorting, microelectrodes have certain technical features that remain attractive in such deep brain stereotactic procedures. Microelectrode recordings without spike sorting can readily enable one to distinguish when one runs out of neurons, and can correlate such events with impedance changes, such as delineating the passage of the electrode ventral to the GPi.[1] Microelectrodes can also provide a thinner alternative to macroelectrodes for stimulation of fragile structures such as the optic tract.

Whether more precise mapping within the GPi by using sensorimotor data would improve localization is not directly addressed in our study of neurons in awake patients at rest. It has been argued that in addition to characterizing GPi cells at rest, sensory and motor mapping information can be used to isolate further the sensorimotor region of the GPi.[18,19] Our observations of neuronal activity during rest do not address the potential utility of active sensorimotor mapping, but searching for the sensorimotor region within the GPi would become considerably more problematic if the framework to outline the borders of the GPi itself were unreliable. In addition, such sensorimotor analyses face some of the same technical difficulties that hamper studies of patients at rest, namely, that identification and differentiation of single neurons online in the operating room can be technically quite error-prone and complex.

Conclusions

In this study of microelectrode recordings obtained within the GP in patients with PD, we have failed to find reliable correlations between neuronal activity and GPe or GPi depth within the GP.

References

1. Alterman RL, Sterio D, Beric A, et al: Microelectrode recording during posteroventral pallidotomy: impact on target selection and complications. **Neurosurgery 44:**315–323, 1999
2. Bair W, Koch C, Newsome W, et al: Power spectrum analysis of bursting cells in area MT in the behaving monkey. **J Neurosci 14:**2870–2892, 1994
3. DeBusk BC, DeBruyn EJ, Snider RK, et al: Stimulus-dependent modulation of spike burst length in cat striate cortical cells. **J Neurophysiol 78:**199–213, 1997
4. DeLong MR: Activity of pallidal neurons during movement. **J Neurophysiol 34:**414–427, 1971
5. DeLong MR, Crutcher MD, Georgopoulos AP: Primate globus pallidus and subthalamic nucleus: functional organization. **J Neurophysiol 53:**530–543, 1985
6. Filion M, Tremblay L: Abnormal spontaneous activity of globus pallidus neurons in monkeys with MPTP-induced parkinsonism. **Brain Res 547:**142–151, 1991
7. Hutchinson WD, Lozano AM, Davis KD: Differential neuronal activity in segments of globus pallidus in Parkinson's disease patients. **Neuroreport 5:**1533–1537, 1994
8. Iacono RP, Shima F, Lonser RR, et al: The results, indications, and physiology of posteroventral pallidotomy for patients with Parkinson's disease. **Neurosurgery 36:**1118–1127, 1995
9. Laitinen LV, Bergenheim AT, Hariz MI: Leksell's posteroventral pallidotomy in the treatment of Parkinson's disease. **J Neurosurg 76:**53–61, 1992
10. Lozano A, Hutchison W, Kiss Z, et al: Methods for microelectrode-guided posteroventral pallidotomy. **J Neurosurg 84:** 194–202, 1996
11. Mandl G: Coding for stimulus velocity by temporal patterning of spike discharges in visual cells of cat superior colliculus. **Vision Res 33:**1451–1475, 1993

12. Miller WC, DeLong MR: Altered tonic activity of neurons in the globus pallidus and subthalamic nucleus in the primate MPTP model of parkinsonism, in Carpenter MB, Jayaraman A (eds): **The Basal Ganglia II: Structure and Function. Current Concepts.** New York: Plenum, 1987, pp 415–427
13. Schaltenbrand G, Wahren W: **Atlas for Stereotaxy of the Human Brain.** Stuttgart: Georg Thieme, 1977
14. Spiegel EA, Wycis HT, Baird HW III: Long-range effects of electropallidoansotomy in extrapyramidal and convulsive disorders. **Neurology 8:**734–740, 1958
15. Sterio D, Beric A, Dogali M, et al: Neurophysiological properties of pallidal neurons in Parkinson's disease. **Ann Neurol 35:** 586–591, 1994
16. Svennilson E, Torvik A, Lowe R, et al: Treatment of parkinsonism by stereotactic thermolesions in the pallidal region. A clinical evaluation of 81 cases. **Acta Psychiatry Neurol Scand 35:** 358–377, 1960
17. Taha JM, Favre J, Baumann TK, et al: Tremor control after pallidotomy in patients with Parkinson's disease: correlation with microrecording findings. **J Neurosurg 86:**642–647, 1997
18. Tsao K, Wilkinson S, Overman J, et al: Pallidotomy lesion locations: significance of microelectrode refinement. **Neurosurgery 43:**506–513, 1998
19. Vitek JL, Bakay RAE, Hashimoto T, et al: Microelectrode-guided pallidotomy: technical approach and its application in medically intractable Parkinson's disease. **J Neurosurg 88:**1027–1043, 1998
20. Wheeler BC: Automatic discrimination of single units, in Nicolelis MAL (ed): **Methods for Neural Ensemble Recordings.** Boca Raton: CRC Press, 1999, pp 61–77

Manuscript received July 3, 2001.
Accepted in final form March 27, 2002.
This work was supported by National Institutes of Health Grant Nos. 7K02MH01493 and 2R01MH50006 to Dr. Schiff.

Address reprint requests to: Steven J. Schiff, M.D., Ph.D., Krasnow Institute, Mail Stop 2A1, George Mason University, Fairfax, Virginia 22030. email: sschiff@gmu.edu.